PHYSICAL REVIEW B VOLUME 22, NUMBER 10 15 NOVEMBER 1980

Direct observation of the behavior of heavy single atoms on amorphous carbon substrates*

M. Utlaut
Enrico Fermi Institute, Department of Physics, The University of Chicago, Chicago, Illinois 60637
(Received 28 March 1980)

Using a scanning transmission electron microscope it is possible, by directly imaging single atoms, to investigate the motion and distribution of heavy (high-Z) atoms deposited on the surfaces of thin low-Z films. In this study, the heavy atoms U, Pt, Au, In, Cd, Ag, and Pd were deposited on 15-Å-thick amorphous carbon substrates. It is found that adatom motion is strongly dependent upon local substrate structure and adatom species. Diffusion coefficients and activation energies for single atoms, as well as dimers, trimers, etc., have been obtained by directly measuring the motion of the atoms. Pair-density and nearest-neighbor distributions were measured and used to derive the interatomic potential and the rate of adatom nucleation. It is found that the interatomic potential is very weak and long ranged.

I. INTRODUCTION

A knowledge of the behavior of single atoms on surfaces is necessary for understanding such phenomena as nucleation, catalysis, crystal growth, and chemisorption. Atoms adsorbed onto solid surfaces have different properties from those of free atoms or atoms in the bulk of a solid; for example, their energy levels are shifted and broadened by the interaction. Experimental determinations of the properties of single atoms on surfaces have been mainly limited in the past to the use of crystalline surfaces which can be formed into suitable emitters for use in the field ion microscope[1] (FIM). Now, however, the scanning transmission electron microscope[2] (STEM) is able to image single atoms on surfaces of either amorphous or crystalline thin films, and information complementary to that from FIM measurements of the motion and distribution of single atoms for adatom-substrate systems can be obtained. In order to obtain high-resolution, high-contrast images of heavy (high-Z) atoms in the STEM, a low-Z substrate is used.

Measurements of the hopping frequency and jump distance of single atoms and clusters of atoms enable activation energies, diffusion coefficients, active binding sites, and surface potential profiles to be determined, while measurements of the spatial distribution of atoms and clusters provide information concerning the active sites for nucleation and a determination of the interatomic potential for adsorbed atoms.

Measurements of heavy atoms adsorbed onto thin amorphous substrates are scarce and have been previously limited by the lack of resolution or by surface contamination. These problems have now been solved by the development of better electron guns and magnetic lenses and by the use of ultraclean procedures in the preparation and handling of specimens.

For these reasons we have initiated studies of the motion and distribution of heavy atoms on these amorphous carbon films. The range of adatom-adsorbate combinations which can be studied in the STEM has been previously discussed.[3] The criterion for visualization of single atoms is found to be

$$Z_{\text{adatom}} \gtrsim (nd\delta^2)^{2/3} Z_{\text{substrate}}, \tag{1}$$

where δ is the electron-beam probe size, n the atomic density, and d the thickness of the substrate. For the 15-Å-thick carbon films used in this study, adatoms capable of visualization have $Z \gtrsim 30$.

In this study we have measured the jump distances and hopping frequencies of several adatoms with $Z \geq 46$ in order to obtain diffusion coefficients and activation energies. We have also measured the pair-spacing density function and the nearest-neighbor distribution function from which the potential of mean force and approximate rate of aggregation can be obtained.

II. EXPERIMENTAL PROCEDURE

All the data were obtained using a STEM which operated at a pressure of $\sim 3 \times 10^{-10}$ Torr (see Fig. 1). The microscope has been described in detail elsewhere[2,4] and consists of a field emission tip with an electrostatic electron gun mounted on a short-focal-length (~1 mm) magnetic lens. The beam can be focused to form a probe as small as 2.4 Å with a current between 10^{-10} and 10^{-12} A. The imaging mode was dark-field elastic, whereby the elastically scattered electrons are collected with high efficiency (60–80%) by the annular detector located behind the specimen. All micrographs were recorded on 35-mm film from a high-resolution CRT and 16-mm film from a television monitor. The time to record each micrograph was 17 sec.

The specimens for this study were heavy atoms placed on thin (~15 Å) evaporated amorphous carbon films. The heavy atoms were applied either by solvent deposition (UO_2Cl_2, UO_2Acetate $\equiv UO_2Ac_2$, $CdCl_2$, $AuCl_3$, $AgCl_2$) or by resistive evaporation (Pt, Au, In, Ag, Pd). Full details of their preparation can be found in Ref. 5.

In this study, the acceleration voltage was 30–35 keV. The microscope was operated in a manner which eliminated phase-contrast effects and reduced the contribution of inelastically scattered electrons to the image.[5,6] The images can be described by the incoherent imaging approximation[6] so that the image intensity for closely spaced atoms (spacing less than the resolution of the microscope) should be additive.

Because the signal from the annular detector is proportional to the scattered electron current, it is possible to measure elastic cross sections from single atoms. We have used a method of determining elastic cross sections similar to that of Retsky[7] in order to demonstrate that our images contain single atoms. In this method, the intensities of atom spots are obtained from micrographs with a densitometer, and upon subtraction of the contribution to the intensity from the carbon film substrate, the resultant intensities are proportional to the collected elastic cross section σ_{coll}. The constant of proportionality is the incident current density onto the atom, and this is easily obtained by recording the intensity of the incident beam on a micrograph by electronically deflecting the beam onto the annular detector. Figure 2 shows histograms obtained from intensity measurements of unnormalized micrographs[8] of atom spots. In each case, there is a lowest value with one or more multiples, which verifies the use of the incoherent imaging approximation in our analysis.

The collected elastic cross section is related to the total elastic cross section by $\sigma_{el} = \sigma_{coll}/\eta$, where η is the efficiency of collection.[7,9]

Using the data from Fig. 2, elastic cross sections from single atoms have been obtained, and we have compared the results with total elastic cross sections for free atoms calculated from recently published tables of scattering amplitudes.[10] The experimentally determined values are in good agreement with theoretical values, as shown in Table I, and we are therefore confident that our images represent individual heavy atoms.

Since the aim of our study is to determine the behavior of atoms on a surface, it is necessary to ascertain how much atom motion is caused by the probe itself. In order to determine the effect of the beam on atom motion, the dose rate of electrons at the specimen was changed and the

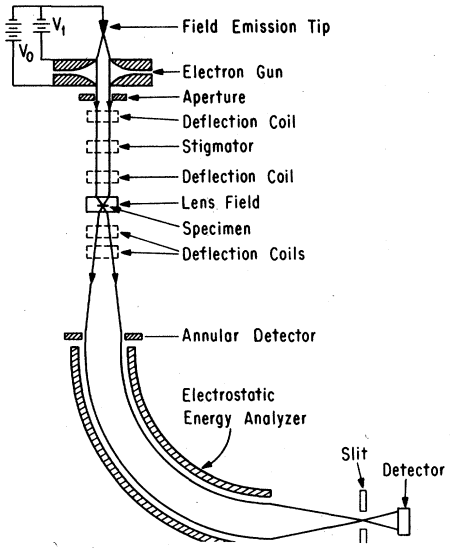

FIG. 1. Schematic diagram of the STEM mounted vertically. V_1 (2–4 kV) and V_0 (20–45 kV) are the emission and acceleration voltages applied to the two-electrode electron gun which produces a highly monochromatic quasiparallel beam of electrons which is focused by the lens to form a probe as small as 2.5 Å. The upper double deflection coils produce the raster scanning on the specimen. The lower deflection coils "unscan" the beam which then passes through the hole in the annular detector. Elastically scattered electrons are collected by the annular detector, inelastically scattered electrons are separated from the unscattered electrons and the remaining elastically scattered electrons. The electrical signals from the detector are used to form an image by modulating the intensity of a synchronously scanned display.

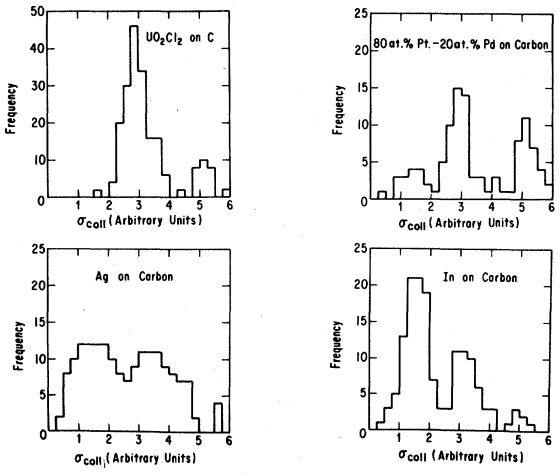

FIG. 2. Histograms of measured intensities of atoms spots from unnormalized micrographs. The intensities are proportional to the collected total elastic cross section. The contribution to the intensity from the film background has been subtracted.

TABLE I. Comparison of measured and theoretical elastic cross sections. The voltage is the acceleration voltage of the electrons. The 20% error is systematic. The number of atom spots measured was 175 U, 62 Pt, 93 In, 85 Ag, and 33 Pd.

	Pd	Ag	In	Pt	U
Theoretical PWA (Å^2)	0.32	0.36	0.37	0.49	0.81
Measured ±20% (Å)	0.31	0.36	0.36	0.48	0.80
Voltage (keV)	34.2	31.2	34.2	34.2	31.2

hopping frequency of the adatoms ν was measured.[3] Figure 3 shows the results of ν when I_0 is changed by nearly two orders of magnitude. Our measurements show that $\sigma_{\text{motion}}/\sigma_{\text{el}} \lesssim 10^{-8}$, and we conclude that our measured frequencies of motion are due to thermal effects.

III. ADATOM MOTION MEASUREMENTS

A. Qualitative observations

Certain aspects of adatom motion are difficult to quantify and we present here some qualitative observations. The motion of heavy adatoms on amorphous carbon surfaces is, in several ways, analogous to adatom motion on crystalline substrates. The motion is strongly dependent on local substrate structure in that most of the motion occurs along ledges separating terraces of different thickenss (see Fig. 4). In some regions, the separation between successive positions of an adatom are integer multiples of 2.4 Å. Diffraction[11] and extended x-ray absorption fine structure (EXAFS)[12] studies of amorphous carbon films (thicker than those used here) indicate that there are regions which are either diamond or graphite, and that the structure may vary with film thickness. We have plotted trajectories of adatoms on certain terrace planes, and judging from the 2.4-Å jump size and the hexagonal structure of the rest sites, these regions may be graphite.[13] The substrates were prepared by arc evaporation onto NaCl at room temperature, and preliminary experiments show that heating during deposition changes the nature of these thin carbon films.[13]

Substrate potential traps exist where adatoms remain during the entirety of our observations (several hours at room temperature), and there are small regions on the surface where diffusing atoms visit more than would be expected from an unrestricted random walk.

There appear to be two types of channeled motion. Single adatoms or pairs of adatoms separated by several Å often migrate in straight lines across apparently smooth terrace planes, or they follow the contours of the edges separating terraces.

FIM studies of diffusion[14,15] have found the discrete random walk to be applicable in describing

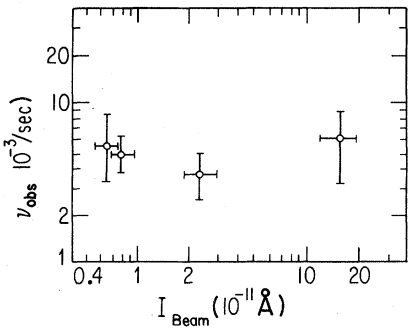

FIG. 3. The observed frequency of motion ν_{obs} of atoms spots for a specimen of uranyl chloride which was solvent deposited on a 20-Å carbon substrate. ν_{obs} was determined by counting the number of atoms which move N_m out of N total atoms per frame time t, i.e., $\nu_{obs} = N_m/Nt$. The horizontal axis is the average beam current during the accumulation of the data. The error bars correspond to the spread in determination of ν_{obs} for each set of observations and the error bars for the beam current correspond to the maximum fluctuations in current during the measurements.

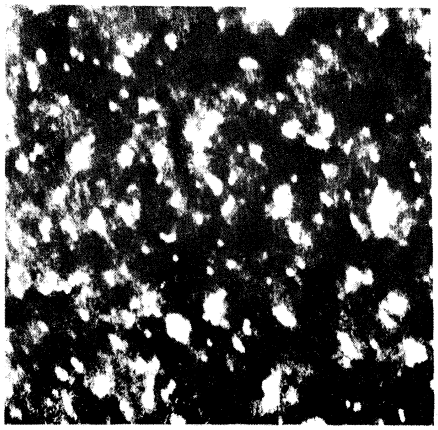

FIG. 4. Micrograph of a typical field of view of the UO_2Cl_2 specimen. The small bright spots are the single uranium atoms, while the larger spots are clusters of unresolved atoms. Variations in background brightness are due to thickness fluctuations in the 15-Å-thick carbon film. The full scale is 235 Å.

adatom motion on crystalline planes, and our observations indicate that the random walk theory is also applicable to motion on amorphous substrates.

For one-dimensional diffusion, the diffusion coefficient D is related to the mean-square displacement d and time t by

$$D=\frac{\langle d^2\rangle}{2t}. \tag{2}$$

For two-dimensional diffusion,[14] this becomes

$$D=\frac{\langle d^2\rangle}{4t}, \quad d^2=x^2+y^2. \tag{3}$$

There are boundary effects in the case of finite planes on which the diffusion occurs.[15,16] The boundaries of the terracelike planes on thin amorphous carbon are usually arbitrary in shape, and dealing with them requires approximations by tractable geometric shapes. It appears that no general statement can be made as to whether these boundaries are reflecting or absorbing.

B. Quantitative results

There are two methods for determining the diffusion coefficient of single adatoms. The first method, which we include here only to demonstrate its applicability, is based on Smoluchowski's theory for the speed of concentration fluctuations.[17,18] In this method, the number of adatoms n_i in a fixed area A is counted at fixed time intervals t. From a series of observations, the mean square successive differences $\langle \Delta^2\rangle_{av}$ can be obtained and for simple geometries, as in the case of a circle of radius r_0, it can be shown[17] that for $r_0^2 > 4Dt$

$$\langle \Delta^2\rangle_{av}=\frac{4\langle n\rangle}{r_0}\left(\frac{Dt}{\pi}\right)^{1/2}. \tag{4}$$

There are two requirements when using this method. The area under observation must be small in comparison to the area of the plane, and must have many adatoms on it. Both of these conditions are satisfied with the specimens used in this study.

TABLE II. Measured diffusion coefficients using Smoluchowski's counting method and the method of direct measurement of atom jump distances.

Adatom	Method	$\langle n\rangle$	D (Å^2/sec)
UO_2Cl_2	Smoluchowski	157	0.014
	Direct		0.016
In	Smoluchowski	190	0.037
	Direct		0.042

The second method involves the direct measurement of the mean-square displacement of individual adatoms and uses Eq. (2) or (3) to obtain the diffusion coefficient. This method also allows the hopping frequency to be measured simultaneously and from this the activation energy for diffusion can be obtained. Table II contains the results of measuring D from the same specimen area by the two methods for an In specimen and UO_2Cl_2 sample. Smoluchowski's method resulted in diffusion coefficients about 15% lower than the direct method, which may be the result of motion preferentially occurring along ledges, which the second method weighs heavily when averaging over the field of observation.

Because the direct measurement of individual adatom motion gives both the diffusion coefficient and the hopping frequency, we have used it rather than Smoluchowski's method. We assume D and ν are governed by the classical rate equation, and depend only on the substrate temperature and the activation energy, as

$$\nu=\nu_0 e^{-E_a/kT}, \tag{5a}$$

$$D=D_0 e^{-E_a/kT}, \tag{5b}$$

where $\nu_0 \approx 10^{13}$ sec^{-1} (kT/h) and D_0 can be obtained once D and E_a have been measured. For a crystalline lattice of constant l, D_0 is usually[19] $\sim kTl^2/h$.

Motion measurements over the entire field of view (~250 Å × 250 Å) give weighted average values of ν and D for the system. A separation of motion data into those atop terraces and along ledge contours shows the effect of substrate structure. Table III gives the results of our measurements of ν, D, and the derived E_a. The results presented in Table III were obtained by tracking at least 75 atoms through no less than 100 frames, except for $AuCl_3$, where 33 atoms were tracked for 60 frames. In all cases, the jump frequency is higher for the adatoms on ledges than that for adatoms migrating on apparently smooth terrace regions. There are instances, however, where we have observed adatoms jumping 15–20 Å across very thin regions of the film which may be only 1–2 atom layers thick. The activation energy for these regions seems to be very low, as adatoms do not bind to them.

Table III also indicates that there is chemical specificity in diffusion in that UO_2Cl_2 shows much less motion and diffusion than UO_2Ac_2. Both molecular species were solvent deposited, and energy-loss spectra obtained from several areas of ~4×10^4 Å^{-2} from both specimens clearly indicate the presence of oxygen, which was not found on a bare 15-Å-thick carbon film. Spectra also show that chlorine remains on the UO_2Cl_2 sample (see Fig. 5), and from cross-section estimates

TABLE III. Measured hopping frequency (ν), diffusion coefficient (D), and the derived activation energy (E_a) obtained from Eq. (5a). The data have been separated into those for the full frame (FF), which is an area of 235 Å×235 Å of the specimen, terraces (T), and ledges (L).

Atom	Site	ν (sec^{-1})	E_a (eV)	D (Å^2/sec)
Ag	FF	5.6×10^{-2}	0.83	0.021
	T	1.2×10^{-2}	0.87	0.016
	L	5.8×10^{-2}	0.83	0.026
$CdCl_2$	FF	8.3×10^{-3}	0.86	0.029
	T	6.9×10^{-3}	0.88	0.026
	L	1.19×10^{-2}	0.87	0.031
In	FF	4.35×10^{-2}	0.84	0.04
	T	1.05×10^{-2}	0.87	0.032
	L	5.6×10^{-2}	0.83	0.044
Au	FF	9.8×10^{-3}	0.88	0.013
	T	6.9×10^{-3}	0.88	0.012
	L	1.2×10^{-2}	0.87	0.014
$AuCl_3$	FF	7.5×10^{-3}	0.88	0.009
	T	6.9×10^{-3}	0.88	0.004
	L	7.7×10^{-3}	0.88	0.011
UO_2Cl_2	FF	5.7×10^{-3}	0.89	0.010
	T	1.1×10^{-3}	0.93	0.005
	L	6.1×10^{-3}	0.89	0.012
UO_2Ac_2	FF	1.6×10^{-2}	0.86	0.036
	T	9.2×10^{-3}	0.88	0.029
	L	2.1×10^{-2}	0.85	0.039

and rudimentary background stripping techniques we estimate that about 50% of the diffusing molecules are UO_2Cl_2.[20-23] The nature of the bonding to the carbon is unknown in these two cases, but it is known that on amorphous carbon, solvent-deposited UO_2Ac_2 can form crystals (containing 7 to ~10^5 atoms), whereas UO_2Cl_2 forms only clusters ~30 Å in diameter which do not appear to be crystalline.[24] Whether chlorine remains on the other specimens deposited as chlorides is not known at this time.

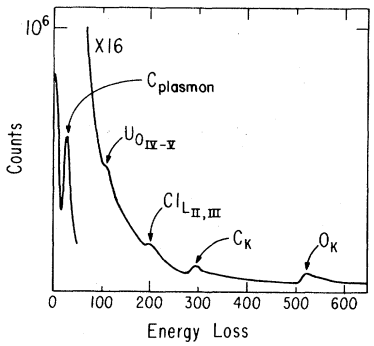

FIG. 5. Electron-energy-loss spectrum of the UO_2Cl_2 specimen. The beam energy was 17 keV, and the probe size was ~200-Å diameter.

The microscope used in this study is not capable of easily changing the substrate temperature, but we have succeeded in cooling the substrate by 10 °C and obtaining diffusion coefficients and hopping frequencies for In and UO_2Cl_2. In both cases the hopping frequency decreased and the results are consistent with Eq. (5a). For the uranyl specimen ν (299.6 K) = $5.7\pm0.2\times10^{-3}$ sec^{-1} and ν (289.5 K) = $1.9\pm0.3\times10^{-3}$ sec^{-1}, while for the In specimen ν (299.6 K) = $4.3\pm0.2\times10^{-2}$ sec^{-1} and ν (290.1 K) = $1.5\pm0.3\times10^{-2}$ sec^{-1}.

From these data at two temperatures, we can

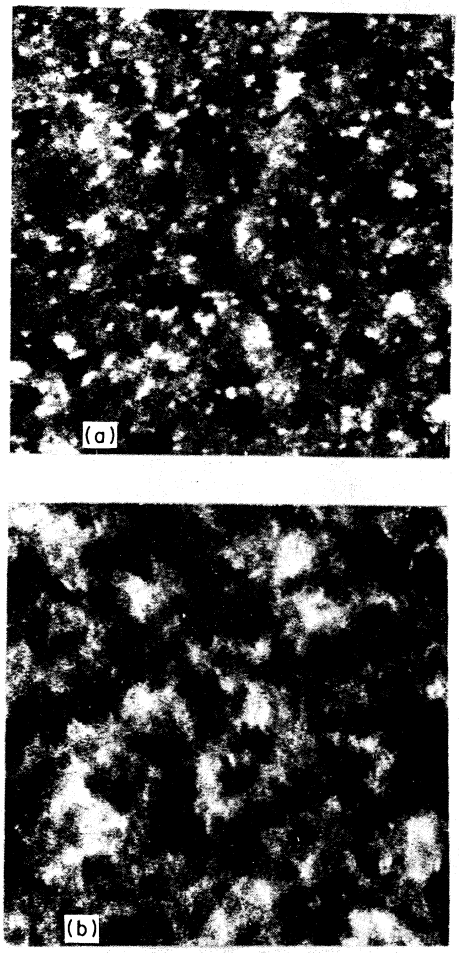

FIG. 6. Micrographs of the In specimen taken a year apart. (a) Shows the specimen several hours after preparation. The single-atom density is 3.21×10^{-3} Å^{-2}. The full scale is 235 Å. (b) Shows the same specimen a year later. Only clusters with 150-Å mean diameter were found. In contrast, the micrograph of Fig. 4 was taken two years after the specimen was prepared.

estimate D_0 and ν_0 from Eqs. (5a) and (5b). Both values of D_0 obtained are reasonable compared to values found from FIM measurements[14,25] of W on W and Rh on Rh, and show that the entropy factor is small for the diffusion of single adatoms at these concentrations. We find for In that $D_0 = 1.2 \times 10^{-(5\pm1.4)}$ cm^2/sec and for UO_2Cl_2 that $D_0 = 2.8 \times 10^{-(4\pm1.4)}$ cm^2/sec. The activation energies derived are consistent with those shown in Table III (for In, $E_a = 0.85$ eV; for UO_2Cl_2, $E_a = 0.87$ eV); and from the hopping frequencies measured at two temperatures, we find from the U data $\nu_0 = 4.9 \times 10^{(12\pm1)}$ sec^{-1}, while from the In data $\nu_0 = 1.5 \times 10^{(12\pm1.4)}$ sec^{-1}.

Micrographs (see Fig. 6) taken nearly a year apart for the two specimens showed that the number and size of the clusters on the UO_2Cl_2 specimen slightly increased (initially there were 1.08×10^{-4} clusters/Å^2 of an average diameter of 15 Å, which after a year changed to 1.5×10^{-4} clusters/Å^2 of 20-Å mean diameter) but that few single atoms remained on the In specimen, as many large (~150-Å diameter) clusters had formed. Clearly, nucleation occurs with more alacrity for In than for UO_2Cl_2.

The activation energies and diffusion coefficients can be easily obtained for dimers, trimers, etc., by tracking them either forward in time from their formation or backward from their dissociation. These quantities are of interest because they must affect transport processes necessary for nucleation to occur.

Table IV shows E_a and ν for dimers for which the individual adatoms were not resolved (i.e., separation ≤ 2.5 Å). The activation energies for $AuCl_3$, $CdCl_2$, and UO_2Cl_2 are nearly equal to those of single adatoms (admolecules), whereas Ag, In, and UO_2Ac_2 dimers have lower activation energies than the singles.

For pairs of adatoms separated by several Å (>2.5 Å), we often see the pair diffuse with an activation energy higher than for the single atoms. For these "dimers," we generally observe that they diffuse by the discrete jump of each atom, and this is reasonable since the simultaneous jumping of two atoms in the same direction is highly unlikely. There is evidence that this picture is valid as we often observe that a restructuring or reorientation of clusters of atoms almost always shows a net displacement of the cluster. The activation energy for diffusion by this mechanism must be influenced by the interatomic potential since a bond has to be stretched during the jumping of an atom. Dimer diffusion of this type should exhibit a frequency factor comparable to that for single-atom diffusion, but with a higher activation energy, given approximately by

$$E_a^{\text{dimer}} = E_a^{\text{single}} + \Delta E_c(r) , \tag{6}$$

where $\Delta E_c(r)$ is the difference in the cohesive interaction energy when the bond is being stretched. Our observations indicate that closely spaced dimers jump more frequently than atom pairs spaced by several Å, possibly because dimer bond formation may withdraw electrons from the region of adatom-substrate bonds. This implies that adatom-substrate interactions are dependent on adatom-adatom interactions. We have seen a general trend that adatoms (on C) which interact more strongly with the surface (i.e., higher E_a) tend to interact more weakly with each other. Equation (6) is then valid as long as the interaction is not weakened by the formation of strong adatom-adatom bonding.

We have also noticed long-range interactions between adatoms. Displacements of a pair of adatoms will not be random if there is an interaction which couples them. For two adatoms on a two-dimensional plane with displacement vectors $\vec{r}_A$ and $\vec{r}_B$ such that

$$\vec{r}_A = \sum_i \vec{r}_{Ai} \quad \text{and} \quad \vec{r}_B = \sum_i \vec{r}_{Bi} , \tag{7}$$

it can be shown that for completely random motion, the mean-square separation between them is the sum of the mean-square displacements of the two adatoms

$$(\vec{r}_A - \vec{r}_B)^2_{\text{random}} = (\vec{r}_A)^2 + (\vec{r}_B)^2 . \tag{8}$$

Following Ayrault and Ehrlich,[25], the observed results can be brought into agreement with the expected values for random motion by introducing a coupling factor C such that

$$(\vec{r}_A - \vec{r}_B)^2_{\text{random}} = C(\vec{r}_A - \vec{r}_B)^2_{\text{measured}} , \tag{9}$$

where $C = 1$ implies uncoupled motion, $C > 1$ implies attractive coupling, and for $C < 1$ the coupling is repulsive. Table V gives values of C for pairs of adatoms on terraces. The C values were derived from observing ten atom pairs in the cases of U and In, seven atom pairs for Cd and Ag, and

TABLE IV. Hopping frequency (ν) and activation energy (E_a) measured for atom dimers separated by ≤ 2.5 Å.

Adatom dimer	ν	E_a
Ag	$\geq 5.90\times10^{-2}$	≤ 0.83
$CdCl_2$	2.29×10^{-2}	0.87
In	$\geq 5.9\times10^{-2}$	≤ 0.83
Au	1.81×10^{-2}	0.86
$AuCl_3$	7.9×10^{-3}	0.88
UO_2Cl_2	6.8×10^{-3}	0.89
UO_2Ac_2	4.34×10^{-2}	0.84

TABLE V. Coupling factors C for pairs of migrating atoms. $C=1$ represents uncoupled motion, $C>1$ represents attractive coupling, and $C<1$ repulsive coupling.

Atom	UO_2Cl_2	Au	In	$CdCl_2$	Ag
Closest approach (Å)	4.3	4.1	9.2	8.6	8.7
Coupling factor C	1.3	16.7	35.2	10.3	19.2

five atom pairs of Au. Again, we observe that UO_2Cl_2 and $AuCl_3$ pairs are uncoupled while In and Ag show the effects of a long-range interaction. The origin of such a long-range interaction may be due to an indirect mediation by the substrate.

CNDO calculations[26] indicate that certain metals are strongly bound to model substrates consisting of graphite, and that the most stable bonding position is at the center of the graphite hexagons. These calculations also indicate that in the case of Ag on C, stabilization occurs when Ag atoms are in contact with other Ag atoms and not in contact with the carbon atoms. Our results for the diffusion of Ag single atoms and dimers are consistent with this notion.

IV. ADATOM DISTRIBUTION MEASUREMENTS

A. Single-atom radial-density function

Another experiment that can be carried out with relative ease in the STEM is the measurement of single-adatom radial density and kth nearest-neighbor distribution functions. Magnification is uniform across the field of view, enabling adatom spacings to be measured with high accuracy by projecting their images, recorded on 35-mm film, onto an x-y digitized scanning table, where the images were enlarged so that the scale on the table was 0.5 Å/mm. Measurements of the coordinates of atoms were made to an accuracy of ~0.25 Å. In order to ascertain observer bias in measuring adatom coordinates, five observers have carried out the measurements for several micrographs, and it was found that the variation among observers is not greater than the variation among several measurements by the same observer ($\leq 5\%$).

The pair and nearest-neighbor distribution functions measured do not include atom spacings for unresolved clusters in the field of view, which remove spacings between 0 and 2.5 Å from the distributions.

The pair-spacing density distribution is defined as

$$\rho(r)=\frac{n(r)K(r)}{2\pi r dr}, \tag{10}$$

where $n(r)$ is the number of adatoms in an annulus of width dr at the distance r from any atom. $K(r)$ is a geometrical correction term which is necessary when the field of view is finite. Figure 7 shows the pair-spacing density functions from typical fields of view from the UO_2Cl_2, Ag, and Cd samples. The horizontal line in each histogram indicates the pair-spacing density for randomly placed adatoms and is given by $\rho_0=n(n-1)/2A$, where n is the number of adatoms in an area A.

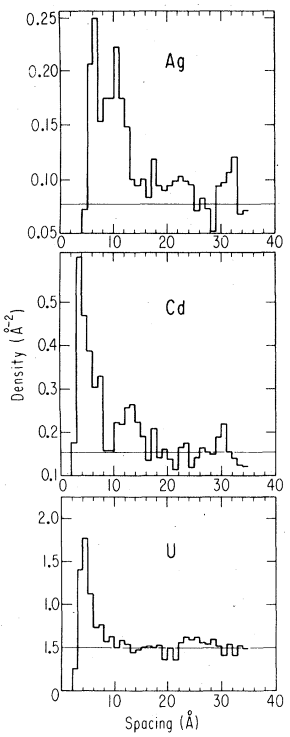

FIG. 7. Histograms of measured pair-spacing density functions. The distributions were obtained by measuring the distances between all resolved single atoms in a 235 Å × 235 Å area of the specimen from enlarged micrographs. The horizontal line in each histogram is the pair-spacing density for randomly positioned atoms.

The pair-spacing densities for these large areas reflect both the irregular structure of the carbon film and adatom-adatom interactions. There is generally a main peak between 3 and 7 Å which depends upon the adatom species and appears to vary slightly with adatom concentration. Uranium compounds are known to form polymer chains of the F-bridge type[27] with a (4–5)-Å spacing between U atoms. Ag, Cd, Au, and In show secondary peaks between 10 and 12 Å, which may result from a long-range adatom interaction. In the case of In, the main peak was observed to continuously grow as a function of time, probably because the speed of nucleation for In is greater than that for the other atoms. Both Ag and Cd show a similar

trend of nucleation, but at rates nearly an order of magnitude smaller. The UO_2Cl_2 pair-density function remained constant over the entire period of observation, as evidently an equilibrium condition had been reached.

There is almost always a smaller broad peak between 25 and 30 Å which reflects the size distribution of the terrace planes. Since most of the adatoms are bound to the interfaces separating terraces of different thickness, this peak is the result of both the intra- and interterrace binding-site distribution.

The pair-density function for several adatoms positioned on a smooth terrace plane can be used to determine the potential of mean force $W(r)$ between adatoms. $W(r)$ is related to $\rho(r)$ by

$$W(r) = -kT \ln \frac{\rho(r)}{\rho_0(r)} , \tag{11}$$

where $\rho_0(r)$ is the pair-density function for noninteracting adatoms.

We have measured $\rho(r)$ for several adatoms (isolated from other adatoms) migrating on smooth terrace planes. Spacings were obtained for five atoms through 100 frames for In and four atoms through 100 frames for UO_2Cl_2, and the results are shown in Fig. 8. Measurements of jump distances indicate that these regions are probably not crystalline. If we assume that $\rho_0(r) = \rho_0$ then $W(r)$ can be obtained from the data of Fig. 8 and is shown in Fig. 9. The points for the first minima have been obtained by approximating the cohesive energy E_c from measurements of the dissociation time t for a dimer[19,28]

$$t \approx \frac{h}{kT} e^{(E_a + E_c)/kT} , \tag{12}$$

and are only order-of-magnitude estimates because Eq. (22) does not properly account for recombination and "configuration weight."[19]

The pair potential $u(r)$ can be closely approximated by $W(r)$ in the low atomic-density limit. The number densities here are small enough for the differences in $u(r)$ and $W(r)$ to be only several percent.[29]

The interatomic potential is very long range and very weak. This observation is valid within the assumptions made and is reasonable for surface atoms as they are more relaxed and their wave functions extend farther than bulk atoms. The existence of two minima and shorter range of $W(r)$ for UO_2Cl_2 may explain the small values of C in Table V and the low rate of nucleation observed.

B. Single-atom nearest-neighbor function

The nearest-neighbor distribution (NND) can be used to obtain the rate of adatom nucleation. A convenient measure of randomness in the NND is the ratio R of measured nearest-neighbor mean distance to the expected distance for a random

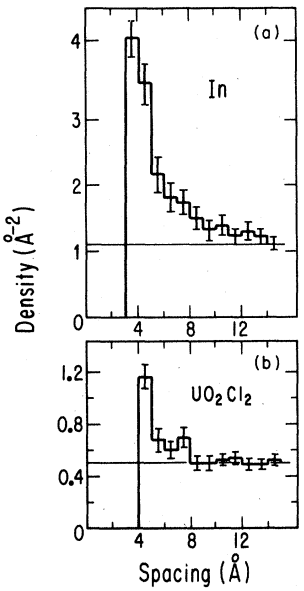

FIG. 8. Histograms of pair-density distribution functions. (a) For five In atoms on a 17-Å radius terrace. (b) For four U atoms on a 19-Å radius terrace.

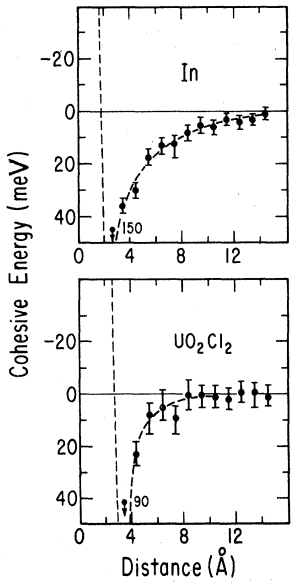

FIG. 9. Cohesive energy derived from Fig. 8. (a) The point at ~ 2.5 Å was obtained by measuring the dissociation time for five dimers; (b) the point at ~ 3.2 Å was obtained by measuring the dissociation time for three dimers.

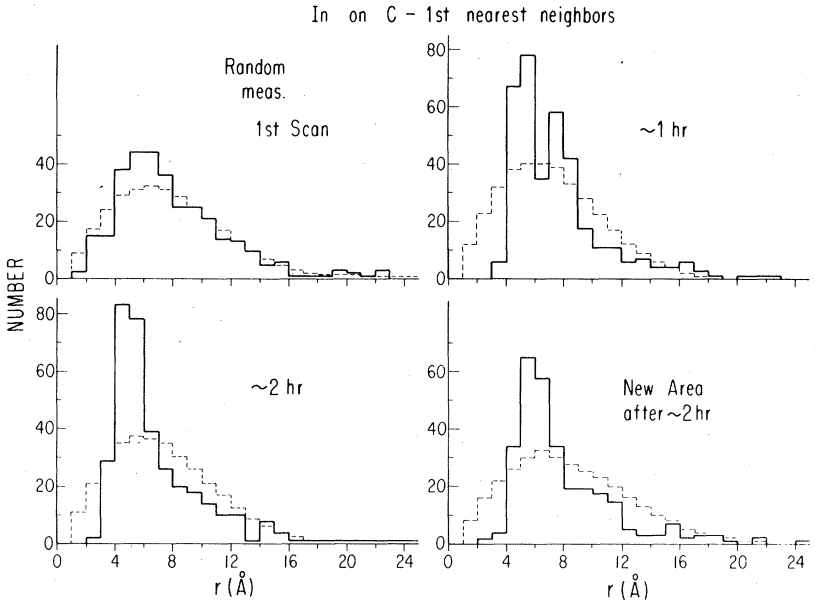

FIG. 10. Histograms of measured nearest-neighbor distributions for single atoms on the In specimen. The solid lines represent the measured values; the broken lines represent calculated random nearest-neighbor distributions. All of the distributions were measured from micrographs representing a 235 Å × 235 Å area of the specimen.

arrangement

$$R=\frac{\langle r_1\rangle_{\text{measured}}}{\langle r_1\rangle_{\text{random}}}. \tag{13}$$

Adatoms randomly positioned on a plane can be described as a Poisson field, and it can be shown[18] that the distribution of nearest neighbors $n_1(r)$ and expected separation $\langle r_1\rangle_{\text{random}}$ depend on the density of adatoms λ as

$$n_1(r)=2\pi\lambda r e^{-\lambda\pi r^2}, \qquad \langle r_1\rangle=\frac{1}{2\sqrt{\lambda}}. \tag{14}$$

$R=1$ implies a random distribution, while $R<1$ implies aggregation. Figure 10 shows the NND for the In sample, and it is clear that from an initially random distribution the mean distance between nearest neighbors is decreasing. The smaller peaks are continuously moving to smaller spacings as time increases, and the main peak is actually more pronounced than shown, because we cannot measure spacings for atoms in unresolved clusters.

In order to show that we are not merely witnessing beam-induced effects, a new area was imaged and the NND measured for the first scan. The new area had slightly fewer atoms, but it is clear that the aggregation process was occurring at about the same rate in the absence of the beam. The time dependence of the NND for UO_2Cl_2 does not show that the adatoms are nucleating. Values of dR/dt are given in Table VI and they are consistent with our motion measurements.

For every case that we have measured, initially adatoms are deposited so that they are randomly positioned, and the rate of nucleation depends upon their mobility (adatom-substrate interaction) and the interaction between adatoms.

C. Clusters

Our observations indicate that generally clusters form near ledges or holes in the substrate. Because we do not have capabilities for *in situ* deposition, our observations take place in the late stages of nucleation.

Figure 11 shows the radial distribution density functions for Pt-Pd clusters and the thinnest regions or holes on the film. For spacings greater than 40 Å, both are randomly distributed. We attribute the absence of smaller spacings to effective accretion areas for cluster formation and nonzero cluster size, which leads to nonoverlap and excludes smaller spacings. From these

TABLE VI. Measured values for $-dR/dT$.

	UO_2Cl_2	Au	In	$CdCl_2$	Ag
$-\frac{dR}{dt}$ (sec^{-1})	~0	$<10^{-7}$	3×10^{-6}	5×10^{-7}	10^{-6}

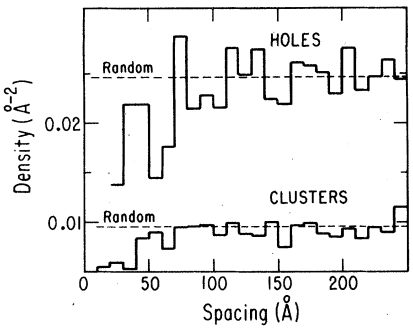

FIG. 11. Histograms of measured pair-density distributions from a 700 Å × 700 Å area of the Pt-Pd specimen. The top histogram represents the distribution of holes and thinnest film regions. The bottom histogram is for the clusters in the field of view.

observations, it appears that active sites for nucleation are randomly distributed.

UO_2Cl_2 clusters show evidence of size instabilities as nucleation attempts to proceed, whereas Ag, Cd, In, and Au appear to be unhindered by size effects. Figure 12 shows two examples of small clusters. The In cluster [Fig. 12(a)] continuously grows with time, while the UO_2Cl_2 cluster [Fig. 12(b)] becomes unstable and eventually breaks apart. We often observe that UO_2Cl_2 clusters reorient into "chains" and then break apart. These examples are not isolated, and are consistent with our observations that the cohesive force for In is larger than that for UO_2Cl_2.

As in the case of dimers, larger clusters show mobility which is several orders of magnitude less than single atoms. Some clusters appear to undergo internal reorientation and in so doing, their center of mass is usually displaced. Certain In clusters containing ~5–15 atoms have been observed to freely migrate until they grow to a size where they are no longer mobile.

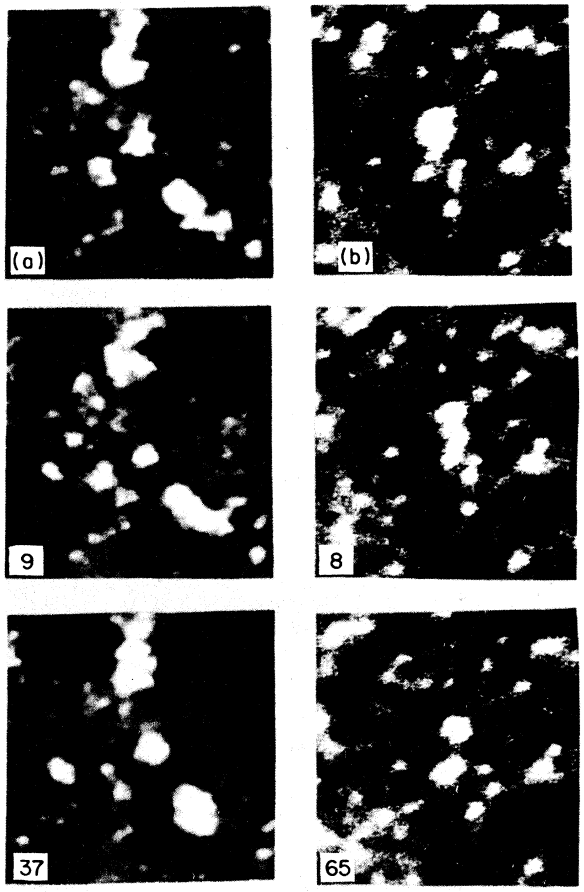

FIG. 12. Micrographs showing clusters. (a) From the In specimen; (b) from the UO_2Cl_2 specimen. The numbers refer to the time in minutes from the first micrograph in each sequence. The full scale of each micrograph is 35 Å.

V. CONCLUSIONS

We have shown that the migration and distribution of heavy atoms in low-Z substrates can be investigated using the 2.5-Å resolution available in the STEM. Images of atoms can be described by the incoherent imaging approximation, and measured elastic cross sections are in agreement with theoretical values and demonstrate that our images contain single atoms. The interaction of the beam with the specimen has been shown to be negligible for producing atom motion, so that the motion we observe is due to thermal activation.

The motion of heavy atoms on amorphous carbon substrates is found to depend on the atom species and the local substrate structure. Correlations in the motion of atom pairs separated by several Å show the existence of long-range interactions, and the potential of mean force derived from measurements of the pair-spacing density function also indicates that surface atoms are weakly attracted at long range.

Future measurements of the behavior of atoms on thin films are necessary. Crystalline support substrates (e.g., graphite) should help to separate adatom-substrate and adatom-adatom interactions from each other, and other low-Z substrates (e.g., Si) should be investigated. A microscope which can easily change the substrate temperature is now being constructed[30] and will enable important measurements of hopping frequencies, diffusion coefficients, and rates of nucleation to be carried out. *In situ* deposition should also prove

interesting in furthering the understanding of the initial-stages of nucleation.

ACKNOWLEDGMENTS

I would like to thank Professor A. V. Crewe for advice and support throughout this work, and the members of his laboratory. This work was supported by grants from the U. S. Department of Energy and the U. S. National Science Foundation.

---

*Submitted in partial fulfillment of the requirements for a Ph.D. from the Department of Physics, The University of Chicago.

[1]E. W. Müller and T. T. Tsong, *Field Ion Microscopy, Principles and Applications* (American Elsevier, New York, 1969).

[2]A. V. Crewe and J. Wall. Optik (Stuttgart) 30, 461 (1970).

[3]M. Isaacson *et al.*, Proc. Nat. Acad. Sci. U.S.A. 74, 1802 (1977).

[4]J. Wall *et al.*, Proc Nat. Acad. Sci. U.S.A. 71, 1 (1974).

[5]M. Ohtsuki, Ultramicroscopy 5, 325 (1980).

[6]J. Fertig and H. Rose, Ultramicroscopy 2, 269 (1977).

[7]M. Retsky, Optik (Stuttgart) 41, 127 (1974).

[8]A normalized elastic signal means that the output of the annular detector is divided by the sum of the signals from all the detectors. In this manner, fluctuations in tip current are not seen. For full details, see, e.g., M. Isaacson, M. Utlaut, and D. Kopf in *Computer Processing of Electron Microscope Images*, Spinger Topics in Applied Physics (Springer, Berlin, 1980), Vol. 13, p. 257.

[9]In order to determine η, we have considered (1) the geometry of the annular detector, (2) the convolution of the convergent incident beam, (3) the effect of spherical aberration of the lens, and (4) contributions from inelastically scattered electrons, bonding, and ionization. The geometry of the detector limits the collection efficiency to 60-80%, while the convergence angle of the beam and spherical aberration are 1-2% effects. Inelastic scattering, bonding, and ionization effects are negligible because of the large angular subtense of the hole in the annular detector.

[10]L. Schäfer, A. V. Yates, and R. A. Bonham, J. Chem. Phys. 55, 3055 (1971).

[11]S. A. Solin and R. J. Koblishka, *Amorphous and Liquid Semiconductors*, edited by J. Stuke and W. Bernig (Taylor and Francis, London, 1973), p. 1251.

[12]P. E. Batson and A. J. Craven, Phys. Rev. Lett. 42, 893 (1979).

[13]M. Isaacson, M. Ohtsuki, and M. Utlaut, in *Proceedings of the 37th Annual EMSA Conference, San Antonio, 1979*, edited by G. W. Bailey (Claitor, Baton Rouge, 1979), p. 498.

[14]See, e.g., G. Ehrlich and F. G. Hudda, J. Chem. Phys. 44, (1964).

[15]T. T. Tsong, J. Chem. Phys. 55, 4658 (1971).

[16]G. Ehrlich, J. Chem. Phys. 44, 1050 (1964).

[17]M. von Smoluchowski, Kolloid-Z 11, 48 (1916).

[18]S. Chandrasekhar, Rev. Mod. Phys. 15, 1 (1943).

[19]T. T. Tsong and P. Cowan, CRC Crit. Rev. Solid State Sci. 7, 289 (1978).

[20]The spectra were obtained in a medium-resolution (200-Å) simple scanning transmission microscope equipped with a high-resolution electron spectrometer. The O_{IV-V} uranium line was detected and the oxygen K line and chlorine L_{II-III} lines were found.

[21]The estimates for cross sections of the O_K, $Cl_{L_{II-III}}$ ionizations were obtained from the curves and parameters in C. J. Powell, Rev. Mod. Phys. 48, 33 (1976).

[22]The estimate for the $U_{O_{IV-V}}$ cross section was extrapolated from the data in C. Wehenkel and B. Gauthe, Opt. Commun. 11, 33 (1974).

[23]R. F. Egerton, Ultramicroscopy 3, 243 (1978).

[24]See, e.g., M. Ohtsuki, Ultramicroscopy, 5, 317 (1980).

[25]G. Ayrault and G. Ehrlich, J. Chem. Phys. 60, 281 (1974).

[26]R. C. Baetzold, Surf. Sci. 36, 123 (1972).

[27]L. Pauling, *The Nature of the Chemical Bond*, 3rd ed. (Cornell University, Ithaca, 1960).

[28]See, e.g., T. T. Tsong, Phys. Rev. Lett. 31, 1207 (1973).

[29]S. A. Rice and P. Gray, *The Statistical Mechanics of Simple Liquids* (Wiley, New York, 1965).

[30]A specimen stage with temperature control is being installed into another atomic-resolution STEM at the University of Chicago; A. V. Crewe (private communication).

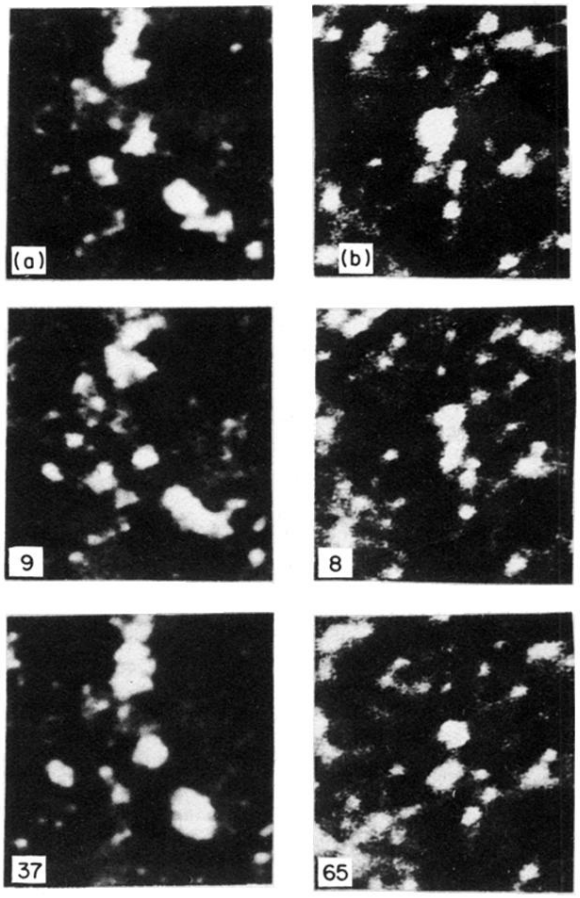

FIG. 12. Micrographs showing clusters. (a) From the In specimen; (b) from the UO_2Cl_2 specimen. The numbers refer to the time in minutes from the first micrograph in each sequence. The full scale of each micrograph is 35 Å.

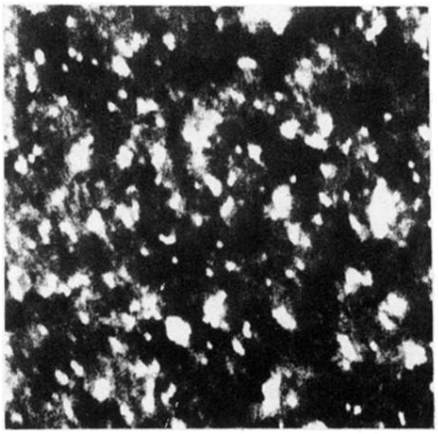

FIG. 4. Micrograph of a typical field of view of the UO_2Cl_2 specimen. The small bright spots are the single uranium atoms, while the larger spots are clusters of unresolved atoms. Variations in background brightness are due to thickness fluctuations in the 15-Å-thick carbon film. The full scale is 235 Å.

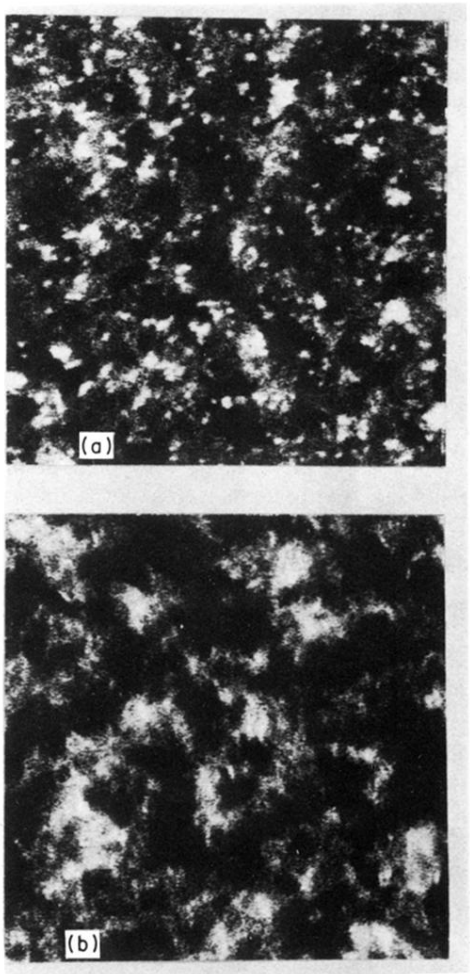

FIG. 6. Micrographs of the In specimen taken a year apart. (a) Shows the specimen several hours after preparation. The single-atom density is 3.21×10^{-3} Å^{-2}. The full scale is 235 Å. (b) Shows the same specimen a year later. Only clusters with 150-Å mean diameter were found. In contrast, the micrograph of Fig. 4 was taken two years after the specimen was prepared.